Lab on a Chip

Accepted Manuscript

ROYAL SOCIETY OF CHEMISTRY

www.rsc.org/loc

Sequential Glycan Profiling at Single Cell Level with the Microfluidic Lab-in-a-Trench Platform: A New Era in Experimental Cell Biology

Tríona M. O'Connell[a,b‡], Damien King[c‡], Chandra K. Dixit[c,d‡], Brendan O'Connor[a,b], Dermot Walls[a,b], Jens Ducrée[c,d]*

It is now widely recognised that the earliest changes that occur on a cell when it is stressed or becoming diseased are alterations in its surface glycosylation. Current state-of-the-art technologies in glycoanalysis include mass spectrometry, protein microarray formats, techniques in cytometry and more recently, glyco-quantitative polymerase chain reaction (Glyco-qPCR). Techniques for the glycoprofiling of the surfaces of single cells are either limited to the analysis of large cell populations or are unable to handle multiple and / or sequential probing. Here, we report a novel approach of single live cell glycoprofiling enabled by the microfluidic "Lab-in-a-Trench" (LiaT) platform for performing capture and retention of cells, along with shear-free reagent loading and washing. The significant technical improvement on state-of-the-art is the demonstration of consecutive, spatio-temporally profiling of glycans on a single cell by sequential elution of the previous lectin probe using their corresponding free sugar. We have qualitatively analysed glycan density on the surface of individual cells. This has allowed us to qualitatively co-localise the observed glycans. This approach enables exhaustive glycoprofiling and glycan mapping on the surface of individual live cells with multiple lectins. The possibility of sequentially profiling glycans on cells will be a powerful new tool to add to current glycoanalytical techniques. The LiaT platform will enable cell biologists to perform many high sensitivity assays and also will also make a significant impact on biomarker research.

Introduction

In this report we present a novel method for sequential cell surface glycoprofiling at a single cell level that allows for the mapping of multiple glycans on a cell's surface. Here we demonstrate the method itself by using a microfluidic LiaT platform. Analysis of the surface glycosylation profile of a single cell is crucial for disease biomarker research in order to correctly elucidate the alteration of expression of a given biomarker[1]. This is important because the abundance of a given biomarker depends on several factors, the most important of which are regulatory molecules, such as chemo/cytokines and an abundance of other biomolecules on neighbouring cells that may affect the biomarker synergistically. Current methods mainly focus on the co-expression of two or more biomarkers, which are an important aspect for prognosis and understanding cell population signalling dynamics. However, this may lead to a loss of specific information about an individual biomarker[2]. Major classes of biomarkers currently employed in disease diagnosis are genetic and proteomic in nature. More recently, glycans or more specifically cell surface glycoproteins have been reported to be excellent early biomarkers for some disease states[3].

Carbohydrates are one of the most abundant, naturally occurring organic molecules; they are central to the synthesis and metabolism of all living systems. Glycans are highly complex carbohydrate molecules and, unlike proteins, they are not encoded directly by the genome[4]. Instead, they are processed and incorporated at specific sites on proteins and lipids in various combinations during post-translational modification by tightly regulated, enzyme-mediated pathways. Their ability to form complexes within themselves and with other biomolecules, such as proteins, makes them a key component of cellular physiology. Examples of glycan-mediated signalling include embryonic development, cell differentiation and growth, cell-cell recognition, contact inhibition and cell signalling. They also have been shown to play a role in immune functions including host-pathogen interactions and appropriate immune response generation[5,6]. Glycans therefore constitute an advanced class of information molecules and the full potential of glycan bio-profiling has yet to be realized.

There are several challenges that must be overcome to further the field of glyco-biology as described in a recent report by the National Academy of Science and Engineering[7,8]. An important challenge is the identification of glycans as potential disease biomarkers, and investigations on their distribution and altered expression between various cell states. A significant hurdle in biological glycoanalysis is the limited availability of glycan-recognition biomolecules. Currently, lectins are the most commonly used probes for glycan analysis. Lectins are proteins that recognise and bind reversibly to specific glycan structures[9]. Although lectin binding affinities for monosaccharaides are generally quite low, they do bind to disaccharides and more complex oligosaccharide structures with significantly higher affinities and exquisite specificity[9]. The binding specificity of lectins can depend not only on specific sugar residues, but also on whether the residue is located at the terminus or within the carbohydrate structure, and on the positions and anomeric configurations (α- or β-) of the linkages between the constituent monosaccharide subunits[9].

The limited repertoire of methods for glycoanalysis is also a major challenge. State-of-the-art glycoanalytical techniques include mass spectrometry (MS), lectin-based methods[10], modified microarrays[11,12], western blotting (protein immunoblotting) and whole cell cytometry methods[13] such as mass cytometry. More recently, glyco-quantitative polymerase chain reaction (Glyco-qPCR) has been developed for the ultrasensitive detection and quantification of glycans in biological samples[14]. Glyco-PCR offers the potential to study low-abundance glycans on cell surfaces and to quantitatively analyse interactions between carbohydrates and proteins that are important for the development and progress of a disease.

However, in spite of the above methodologies, glycan profiling of individual cells is not yet possible due to the limited amount of sample involved; analytical techniques such as microarrays and mass spectrometry need concentrated and high purity glycan fractions which are usually prepared by lysis and concentration of the glycoprotein extracts from a cell population. Thus the potential for single cell resolution and the identification of heterogeneity within the sample are lost. Flow Cytometry or

Fluorescence Activated Cell Sorting (FACS) demands a comparatively large number of cells (usually 50,000 - 100,000), and recovery and identification of individual cells for sequential analysis is again not possible. In addition cells are either destroyed (mass spectrometry, mass cytometry, Glyco-qPCR and microarray) or are subjected to large hydrodynamic shear forces (FACS and microarray). Therefore, these techniques are not appropriate for sequential lectin-based glycoanalysis. Furthermore, and most importantly, the samples involved are usually non-recoverable (**Table 1**). Glyco-qPCR is limited to glycans with a free reducing end and a carboxyl group[14]. Although these properties are common in N-glycans, O-glycans, and glycosaminoglycans, some glycans lack carboxyl groups. The various drawbacks to established methods for extensive glycoprofiling at the single live cell are summarised in **Table 1**.

In this paper we present a novel method of lectin-based glycoanalysis with single cell resolution by the use of a microfluidic LiaT platform[15,16]. This analytical approach for the first time permits repeated probing of the cell surface glycome through the sequential binding and elution of a series of labelled lectins. The key problems that are addressed by employing this approach are:

(i) Glycan profiling of live cells either requires many thousands of cells (FACS) or is restricted to probing only one glycan per cell (microarray). We address this issue by using a LiaT platform that allows for the sequential introduction of reagents by regulating the fluid properties in the microchannels in a low-volume (4 nL), shear-free platform. Thus, using LiaT allowed us to handle smaller cell samples and to deliver low-affinity reagents to the cell surface under vanishing flow field, both prerequisites for the successful implementation of the developed glycoprofiling method.

(ii) The binding of multiple lectins on the cell surface at the same time may result in inaccuracies due to inter-lectin steric hindrance. We address and eliminate this issue by sequentially probing glycans one after another using one lectin at a time. The ability to exchange lectins through sequential elution reduces the problem of steric hindrance between two adjacent binding sites.

(iii) The specificity of lectin binding on the cell surface is confirmed by a reduction in the level of cell-bound fluorescence following elution with the corresponding lectin-specific monosaccharide.

(iv) The cost of analysis can be significantly reduced through the use of a single fluorophore for all lectin types, thereby permitting analysis with a very basic fluorescence microscopy setup. The LiaT system does not require any specialist pumps or other auxiliary equipment. The simple architecture allows cost-efficient mass manufacture of the microfluidic chips.

Furthermore, it has been demonstrated that our method and the LiaT platform can be employed for several other applications[17]. In summary, we show that the LiaT-based multi-lectin technology described here is a significant advance that enables glycan profiling at the level of a single live cell.

Theory

Principles of Lab in a Trench

Lab-in-a-Trench (LiaT) is a microfluidic platform previously developed by Dimov et al. [15,16] in which cells are contained and analysed in a shear-free environment. We reasoned that LiaT would permit glycoprofiling at a single cell level. Several other single cell analysis platforms are available, including constricted channel-based[18], cup-based[19], and cylindrical trap-based systems[20]. Most of these alternative (non-LiaT) systems are either shear-based, continuous flow-based or open (several cell traps in a given area) systems. It has been well established that even slight alterations in biophysical conditions, including hydrodynamic forces, can trigger changes in cellular morphology and physiology[21]. As the LiaT system allows the merely diffusion-based delivery of lectins, cells can be probed in a shear-free environment.

The LiaT platform contains a deep, micron-scale indentation within a continuous channel that enables the capture and retention of cells purely based on gravity [15,16] (**Fig. 1**). LiaT follows a well-known working principle that is based on the Camp-Hazen model of a settling basin[22]. In this model, the velocity of cells over the trench is the most critical parameter for ensuring their gravity-driven capture.

Lab in a Trench - Microfluidic Theory

We consider particle trapping in the trench according to the ***critical trajectory model*** for a Camp-Hazen type settling tank (**Fig. 1a)**. Cells are suspended in a flow of PBS buffer of density $\rho = 1.0 \times 10^3$ kg m^{-3} and viscosity $\eta = 1.09 \times 10^{-3}$ Pa s under the impact of the gravitational acceleration $g = 9.81$ m s^{-2}. A pressure head $\Delta p = 1.5$ hPa built up by a pipette filled to a liquid level $\sigma = 1.5$ cm applies across the main channel has total length $l_{\mathrm{channel}} = 14$ mm, constant height $h_{\mathrm{channel}} = 35$ µm and width $w_{\mathrm{channel}} = 40$ µm which broadens to $w_{\mathrm{trench}} = 250$ µm above the trench of stream-wise length $l_{\mathrm{trench}} = 100$ µm (**Fig. 1b**). Neglecting the trench section, the (average) flow of velocity then amounts to

$$v_{\mathrm{channel}} = \frac{h_{\mathrm{channel}} w_{\mathrm{channel}} \Delta p}{C_{\mathrm{nc}} \eta l_{\mathrm{channel}}} \approx 430\,\mu\mathrm{m\,s}^{-1}$$

with the numerical coefficient for the rectangular channel $C_{\mathrm{nc}} \approx 32.14$. The (average) flow velocity even reduces to

$$v_{\mathrm{trench}} = \frac{w_{\mathrm{channel}}}{w_{\mathrm{trench}}} \cdot v_{\mathrm{channel}} \approx 70\,\mu\mathrm{m\,s}^{-1}$$

within the sector above the trench. The resulting Reynolds number

$$\mathrm{Re} = \frac{\rho v w}{\eta} << 1$$

indicates that flow conditions are strictly laminar within the channel as well as in the trench for typical flow speeds v and widths w. Hence, streamlines will only penetrate into the uppermost region of the trench and molecular (reagent) transport across streamlines into the trench occurs solely through diffusion[15] (**Fig. 1a**).

With the speed of sedimentation

$$v_{\text{sed}} = \frac{g d^2}{18\eta}\left(\rho_{\text{cell}} - \rho\right)$$

for cells of density ρ_{cell} and diameter d we can determine the ratio

$$\frac{t_{\text{sed}}}{t_{\text{in}}} = \frac{18\eta\, h_{\text{channel}}}{g\, d^2\left(\rho_{\text{cell}} - \rho\right)} \cdot \frac{v_{\text{channel}}}{\left(l_{\text{channel}}/2\right)}$$

between the sedimentation time t_{sed} (h) = h_{channel} / v_{sed} across the entire channel height h_{channel} and the (minimum) residence time of the cells in the incoming segment t_{in} = 0.5 l_{channel} / v_{channel} located at about 0.5 l_{channel} after the inlet. For Ramos cells with a density of $\rho_{\text{cell}} = 1.02 \times 10^3$ kg m^{-3} and a typical diameter d = 10 µm suspended in PBS buffer, this ratio is much smaller than unity so that the entire population of Ramos cells will have settled to the bottom of the channel way before reaching the downstream trench (**Fig. 1b**).

Due to the parabolic flow profile, their speed of cell migration will hence be significantly reduced with respect to the above calculated (average) flow velocity v_{trench}. The cell velocity in the trench region

$$v_{\text{cell}} \approx 2v_{\text{trench}}\left(\frac{h_{\text{cell}}}{h_{\text{channel}}/2}\right)^2 = 8v_{\text{channel}}\frac{w_{\text{channel}}}{w_{\text{trench}}}\left(\frac{h_{\text{cell}}}{h_{\text{channel}}}\right)^2$$

depends on the distance of the cell from the bottom of the channel h_{cell}. If, for instance, a cell was touching the bottom of the channel (**Fig. 1b**), i.e. $h_{\text{cell}} = d / 2$, their speed of horizontal migration would amount to $v_{\text{cell}} \approx 10$ µm s^{-1}, only.

For efficient trapping, the ratio

$$\frac{t_{\text{sed}}}{t_{\text{res}}} = \frac{18\eta h}{g d^2\left(\rho_{\text{cell}} - \rho\right)} \cdot \frac{v_{\text{cell}}}{l_{\text{trench}}} \approx \frac{18\eta h}{g d^2\left(\rho_{\text{cell}} - \rho\right)} \cdot \frac{2v_{\text{channel}} w_{\text{channel}}}{w_{\text{trench}} l_{\text{trench}}}\left(\frac{d}{h_{\text{trench}}}\right)^2 < 1$$

of the cell sedimentation time (to a depth d into the trench) and the cell residence time in the trench region needs to be lower than unity. This implies an upper limit

$$v_{\text{channel}}{}^{*} = \frac{g(\rho_{\text{cell}} - \rho) w_{\text{trench}} l_{\text{trench}} h_{\text{trench}}{}^2}{36\eta h w_{\text{channel}}}$$

for the flow speed in the (main) channel. Assuming that the cell will be irreversibly trapped after penetrating a distance corresponding to the channel height into the trench, i.e. $h = h_{\text{channel}}$, we obtain a speed limit of $v_{\text{channel}}{}^{*}$ = 545 µm s^{-1} > v_{channel} = 430 µm s^{-1} as calculated above. Please note that while the derived equations are quite instructive for the understanding of the system and we

even obtain a speed limit compliant with an experimentally observed flow rate at which trapping occurs, these "back-of-the-envelope" calculations are just coarse, order-of-magnitude estimates in a more quantitative picture.

COMSOL Simulations

Liquid flow profiles (**Fig. 1a**) obtained for channels of these dimensions have been comprehensively simulated by COMSOL modelling[15].

Lab in a Trench - Micro-Fabrication

The platform is a two layer polydimethylsiloxane (PDMS) system whereby a lower PDMS panel holds structures (channel and trenches), while an upper panel has reservoirs. In brief, PDMS (Dow Corning) was mixed with curing agent in a ratio of 5:1 for the trenches and 20:1 for the lid, followed by degassing for a minimum of 30 min under vacuum. Degassed PDMS was then poured on the appropriate silicon masters and partially cured for 3-4 hours at room temperature under vacuum. Inlet holes (diameter: 1 mm) were then punched in the lid structure. The two PDMS layers containing the channels and reservoirs were then aligned, bonded and cured at 70^{o}C for 24 hours.

Gravity Driven Flow

Gravity driven flow was implemented by fitting a vertically aligned, standard pipette tip in the inlet hole of the LiaT chip and loading it with input fluid. The flow velocity was determined by the height of the liquid column which was kept at roughly σ = 1.5 cm over the course of the experiment.

Device Priming and Cell Loading

The fabricated LiaT was O_2 plasma treated for 5 min. Then channels and trenches were immediately primed with 100-mM Tris-buffered saline (TBS), pH = 7.4, containing 1 mM $CaCl_2$. Each inlet was then loaded with cells by adding 0.4 µl of culture (10^5 cells per mL) to the 20 µL of TBS already present in the gravity pump.

Capture efficiency close to 100% was routinely achieved within the system by keeping the flow velocity at the inlet within the range of ≤ 430 µm s^{-1} and ensuring that the channel to trench depth ratio was kept above 1:5. It has been shown by Manbachi *et al*. that a shear stress-free environment exists within the trench under such conditions[23] and, as a consequence, flow velocities are at least three times lower at the bottom of the trench relative to the top[15, 23].

Three times the required number of cells to be captured was loaded. By operating in the critical flow velocity range of ≤ 430 µm s^{-1}, the required number of cells can be captured in the trench. Surplus cells were then removed by increasing the flow

velocity (> 430 μm s^{-1}) at the inlet and these then passed over the top of the trench and travelled to the waste chamber at the bottom of the chip.

Briefly, Ramos cells were suspended in TBS buffer by adding ~1,500 cells to a 20 mL solution of TBS. Cell suspensions and reagents were loaded and pumped through the system with a hydrostatic pressure-head[17] created by liquid level in the pipette tip. Theoretically, a trench can hold approximately 60 non-overlapping cells and up to 200 cells if there is no requirement for such a monolayer. Reagents were introduced at higher speeds to establish a fixed concentration on top of the trench. The laminar flow in the channel ensured an abruptly vanishing flow field below the plane of the upper flow channel, i.e. essentially throughout the entire trench (**Fig. 1**). Therefore, shortly after the cells have entered the trench, they are irreversibly retained in a flow-free environment; as they maintain their location at the bottom of the trench and can hence be individually observed over time. Access of reagents and wash buffer to the trench-trapped cells therefore solely occurs by diffusion and so the hydrodynamic stress to which these captured cells are exposed, are negligible. In addition, trench depths as small as 200 μm (with typical volumes of 4 nL) allow continuous loading of reagents and nutrients to provide efficient on-chip cell culturing.

Experimental

Reagents

Biotinylated lectins (WGA, ConA, ECL, LCA, NPL) were obtained from Vector Laboratories. These were labelled with DyLight 488 - streptavidin (Vector Laboratories) according to the manufacturer's instructions. Fucose, mannose, galactose and N-acetyl-glucosamine were purchased from Sigma. All lectins and sugars were suspended in TBS pH 7.4 with 1 mM $CaCl_2$.

Cell Culture

Ramos cells (ATCC no. CRL-1596), a B cell line of Burkitt's lymphoma origin, were cultured in RPMI 1640 (Sigma) supplemented with 10% heat inactivated foetal calf serum (Gibco) and 1% penicillin / streptomycin (Sigma). Cells were incubated at 37°C with 5% CO_2, split every two to three days and seeded at a density of 2.5×10^5 cells ml^{-1}.

Sequential Glycan Profiling

Each Dylight488-conjugated lectin (1 μl of 0.1 mg mL^{-1}) was introduced in the inlet with 20 μl buffer reserve. The lectin flows with the buffer in the channel. The typical time for the (near) completion of lectin diffusion from the inlet to the bottom of the trench was 20 s. Lectin binding to cells was monitored by fluorescence microscopy every 5 min. After reaching binding saturation, which was different for each lectin, free sugar (20 μl of buffer with 2 μL 1M sugar giving a working concentration of 100 mM) was introduced into the system to elute bound lectin from the cell surface (**Fig. 2)**. Elution sugar was chosen according to the

specificity of each lectin as shown in **Supplementary Table 1**. The elution sugar of a preceding lectin does not hinder the binding of the next incoming lectin unless both lectins have an affinity for the same sugar. In this case, the liquid in the system was replaced with fresh TBS. LCA, ConA and NPL bind specifically to mannose and its derivative arrangements, thus in those cases there was a need to change inlet buffer after each elution.

Fluorescence Microscopy

The trench was imaged with an Olympus IX81 motorized inverted microscope with an attached Hamamatsu ORCA - ER digital camera C4742-80 using a 10X objective. The microscope platform was maintained at 5% CO_2 and a temperature of 37^{o}C for the duration of the experiments. After the introduction of each lectin into the channel, focus was maintained on the cells for the duration of each lectin binding and elution event. Images were captured at that focus after 5 min in TIFF format in order to preserve the original pixel densities of the image (**Fig. 2)**.

Image Analysis with ImageJ

Images were analysed by the software ImageJ (version 1.46r). Fluorescence intensity was quantitated by 'region of interest (ROI)' analysis. An average intensity was obtained for each cell through the time series. Fluorescent images of the final time point of each lectin series were used to create overlays of individual cells. This allowed a visual depiction of the glycan distribution across the surface of the cells. Examples of the overlaid images are shown in **Figs. 3b, 4b and 5b**.

Results and Discussion

Sequential Glycan Probing

The LiaT platform was employed to examine the surface glycosylation of Ramos B lymphoma cells, and benchmarked with characterization of the same features by flow cytometry (**Supplementary Fig. 1).** Ramos cell surface glycans were thus sequentially probed by a panel of four fluorescently-labelled lectins, categorized as mannose- (LCA, NPL and ConA), galactose- (ECL) and N-acetylglucosamine- (GlcNAc) binders (WGA). A summary of the sequential experiments undertaken is presented in **Table 2**. The interference of free sugar from previous stains was assessed with three mannose-binding lectins, namely, LCA, ConA and NPL (**Supplementary Table 1**). An additional wash step was incorporated between sugar elution and addition of the next lectin in the sequence.

Each trench was loaded with 15-20 cells in TBS with 1 mM $CaCl_2$. Each DyLight488-labelled lectin was introduced in the LiaT at a concentration of 11 μg μL^{-1} and diffused to the cells at the bottom of each trench in less than 30 s, as also shown to be the case in the COMSOL simulations performed by Dimov *et al*.[15] The resultant lectin concentration effectively available for cells to bind was

therefore 13 pg in each 4-nl trench. Lectin-binding events were then recorded over time by epi-fluorescence microscopy. They are presented here in 5-min time steps (**Figs. 3 – 5**) as a function of increasing fluorescence signal until saturation established. This was followed by elution with the specific sugar substrate of the bound lectin. A summary of the different sequential profiling experiments performed is given in **Table 2**.

In the first experiment with the two lectins LCA and ECL, stronger signals were detected with LCA indicating a denser mannose distribution at the cell surface when compared to ECL, which has an affinity for galactose residues (**Fig. 3**). This is in agreement with general cell surface glycan structures because galactose is known to be either protected or partially exposed on live healthy cells which results in poor ECL binding and hence lower equilibrium concentrations and reduced signals[24].

In a second experiment involving three mannose-binding lectins, the successive binding of the second and third lectins was not affected by the presence of mannose during earlier steps in the probing sequence, i.e. indicating the effectiveness of the preceding wash step (**Fig. 4)**. The peak fluorescence of LCA and ConA was comparable to those achieved in the next experiment (**Fig. 5)** also including ConA and WGA. In this 4-lectin experiment, a higher signal was obtained with the latter and an intermediate signal with the former (**Fig. 5**). This experiment confirmed high GlcNAc and core mannose levels on the cell surface. When mannose binders (LCA and ConA) were compared, the amount of bound LCA was found to be lower than that of bound ConA. This is likely to reflect the known difference in affinity between LCA and ConA, where the former only recognizes α-linked fucosylated mannose. GlcNAc presented with the highest density among all the exogenous glycans that were probed.

As the lectins were added in an order such that sugar elution would not interfere with the following lectin, we were able to image individual cells without the requirement for wash steps. This allowed us to create spatio-temporal glycan density profiles of the cell surface using regular image analysis (**Supplementary Fig. 2**). In addition, the order of lectins was selected so as to minimise impact on the cells, based on the changes observed when using each lectin in flow cytometry (**Supplementary Fig. 1**). The sugar elution steps were rapid (in the order of minutes), thus minimising any potential physiological impact on the cells in the trenches. It can be noted that in experiments 2 and 3, LCA was followed directly or indirectly by ConA (**Figs. 4 and 5)**. In experiment 3, similar observations were made to experiment 2, indicating that the fucose elution of ECL in experiment 3 had not interfered with the cells' binding of ConA.

Qualitative Cellular Glycan Map

Through the software Image-J we have generated a qualitative glycan map by simple co-localisation of individual lectins and an overlap of all bound lectins (**Figs. 3b, 4b and 5b**). In general, a cell population was profiled at successive points in time and the resulting images were then overlaid with computational tools to produce the glycan map.

In-Trench Lectin Specificity

We have confirmed that the free sugars can be washed from the system such that they do not interfere with the following lectin. This has been demonstrated by targeting a common carbohydrate (mannose in this case) with three different lectins (LCA, ConA and NPL) that probe mannose and exhibit similar specificities. We found binding of all lectins to similar positions on the cell surface but with varying intensities (**Fig. 4b**).

Heterogeneity Analysis: Single Cell versus Cell Population

The results generated were then analysed with a view to understanding glycan heterogeneity at the single-cell level. An difference was observed at the inter-cellular (n = 12) level in the glycan-probing behaviours of lectins on individual cells as demonstrated by their NPL lectin profile (**Supplementary Fig. 3**). Lectins are usually low-affinity binders with their dissociation rate constants (K_d) ranging from 10^{-4} to 10^{-7} mol^{-1} s^{-1}. The impact of glycan structure and complexity has been known for a long time but its functional interpretation has only begun to be addressed in the last few years[25-27].

The sequential lectin-elution method has thus enabled us to detect multiple sugars over time on a given live cell and that is a considerable technical advancement over current state-of-the-art methods. We show here that the LiaT platform also permits the differential characterization of diverse glycosylation features at the single cell as well as at a population level. By overlaying the images of different lectin probes, one could also effectively perform various other qualitative and quantitative analyses like the kinetics of lectin binding to cell-bound sugars and the development of sugar distribution profiles (**Supplementary Fig. 4**). Coupled to LiaT platforms, this strategy has the potential to significantly impact on the advancement of glycoanalysis.

Conclusions

Due to minimisation of cell translocation as well as alterations to the physiological dynamics at their surface, the sequential binding of lectin probes to glycans on the surface of individual cells within a population can be analysed the novel LiaT platform. Furthermore, the simple geometry allows very cost-efficient mass manufacture. Beyond the here presented application in glycoscience, the LiaT platform thus also bears a significant potential to expand the analytical toolbox of cell biology and biomarker discovery.

Notes and references

1. S. J. Altschuler and L. F. Wu, *Cell*, 2010, **141**, 559–63.

2. V. Almendro, A. Marusyk, and K. Polyak, *Annu. Rev. Pathol.*, 2013, **8**, 277–302.

3. D. H. Dube and C. R. Bertozzi, *Nat. Rev. Drug Discov.*, 2005, **4**, 477–88.

4. A. Varki, R. D. Cummings, J. D. Esko, H. H. Freeze, P. Stanley, C. R. Bertozzi, G. W. Hart, and M. E. Etzler, Eds., *Essentials of Glycobiology*, Cold Spring Harbor Laboratory Press, Cold Spring Harbor(NY), 2nd Editio., 2009.

5. K. Ohtsubo and J. D. Marth, *Cell*, 2006, **126**, 855–67.

6. H. Ghazarian, B. Idoni, and S. B. Oppenheimer, *Acta Histochem.*, 2011, **113**, 236–47.

7. National Academy of Sciences National Academy of Engineering Institute of Medicine National Research Council, *Transforming Glycoscience: A Roadmap for the Future*, 2012.

8. J. F. Rakus and L. K. Mahal, *Annu. Rev. Anal. Chem. (Palo Alto. Calif).*, 2011, **4**, 367–92.

9. M. Ambrosi, N. R. Cameron, and B. G. Davis, *Org. Biomol. Chem.*, 2005, **3**, 1593–608.

10. J. Hirabayashi, A. Kuno, and H. Tateno, *Electrophoresis*, 2011, **32**, 1118–28.

11. A. Kuno, N. Uchiyama, S. Koseki-Kuno, Y. Ebe, S. Takashima, M. Yamada, and J. Hirabayashi, *Nat. Methods*, 2005, **2**, 851–6.

12. H.-H. Jeong, Y.-G. Kim, S.-C. Jang, H. Yi, and C.-S. Lee, *Lab Chip*, 2012, **12**, 3290–5.

13. D. R. Gossett, W. M. Weaver, N. S. Ahmed, and D. Di Carlo, *Ann. Biomed. Eng.*, 2011, **39**, 1328–34.

14. S. J. Kwon, K. B. Lee, K. Solakyildirim, S. Masuko, M. Ly, F. Zhang, L. Li, J. S. Dordick, and R. J. Linhardt, *Angew. Chem. Int. Ed. Engl.*, 2012, **51**, 11800–4.

15. I. K. Dimov, G. Kijanka, Y. Park, J. Ducrée, T. Kang, and L. P. Lee, *Lab Chip*, 2011, **11**, 2701–10.

16. G. Kijanka, R. Burger, I. K. Dimov, R. Padovani, K. Lawler, R. O'Kennedy, and J. Ducrée, *Advanced Biomedical Engineering*, InTech, 2011.

17. I. K. Dimov, G. Kijanka, and J. Ducree, in 2010 IEEE 23rd International Conference on Micro Electro Mechanical Systems (MEMS), IEEE, 2010, pp. 96–99.

18. A. C. Rowat, J. C. Bird, J. J. Agresti, O. J. Rando, and D. A. Weitz, *Proc. Natl. Acad. Sci. U. S. A.*, 2009, **106**, 18149–54.

19. A. M. Skelley, O. Kirak, H. Suh, R. Jaenisch, and J. Voldman, *Nat. Methods*, 2009, **6**, 147–52.

20. L. Lin, Y.-S. Chu, J. P. Thiery, C. T. Lim, and I. Rodriguez, *Lab Chip*, 2013, **13**, 714–21.

21. S. Elliott, *Cell Damage due to Hydrodynamic Stress in Fluorescence Activated Cell Sorters*, The Ohio State University, 2009.

22. N. M. C. Saady, *J. Appl. Sci. Environ. Sanit.*, 2011, **6**, 309–15.

23. A. Manbachi, S. Shirvastava, M. Cioffi, B.G. Chung, M. Moretti, U. Demirchi, M. Yliperttula and A. Khademhosseini, *Lab Chip*, 2008, **8**, 747-754.

24 H. Tateno, N. Uchiyama, A. Kuno, A. Togayachi, T. Sato, H. Narimatsu, and J. Hirabayashi, *Glycobiology*, 2007, **17**, 1138–46.

25. N. Sethuraman and T. A. Stadheim, *Curr. Opin. Biotechnol.*, 2006, **17**, 341–6.

26. J.-T. Cao, Z.-X. Chen, X.-Y. Hao, P.-H. Zhang, and J.-J. Zhu, *Anal. Chem.*, 2012, **84**, 10097–104.

27. J. Hirabayashi, M. Yamada, A. Kuno, and H. Tateno, *Chem. Soc. Rev.*, 2013, **42**, 4443–58.

[a] *School of Biotechnology, Dublin City University, Glasnevin, Dublin 9, Ireland*
[b] *Irish Separation Science Cluster, Dublin City University, Glasnevin, Dublin 9, Ireland*
[c] *School of Physical Sciences, Dublin City University, Glasnevin, Dublin 9, Ireland*
[d] *Biomedical Diagnostics Institute, National Centre for Sensor Research, Dublin City University, Glasnevin, Dublin 9, Ireland*

*Corresponding author: Email: jens.ducree@dcu.ie; Phone: **+353 1 700 7870;** Fax: **+353 1 700 7873**

‡ Authors contributed equally

Glycoprofiling strategies	Limitations	Advantages	Ref
Whole cell-based approaches			
Flow cytometry	• Requires huge number of cells • Works at population level • Costly instrumentation • Inability to localise multiple glycans on cell surface and on protein domains • Cells are exposed to tremendous pressures that may induce changes leading to false characterization • Inability to correlate the retrieved cells to their FACS data for further validation	• High-throughput and quantitative • Routinely employed in clinical set-ups and industries	6-8
Microscopy	• Inability to perform multi-lectin glycoprofiling • Multiple staining is laborious with a high probability of inter-stain steric hindrance	• Possible to localise glycans on cell surface	9
Crude cell lysate-based approaches			
Microarray	• Homogeneous cell population required • Inability to classify sub-populations • Inability to allow single cell multi-lectin glycoprofiling • Expensive, labour-intensive • High detection limits and narrow detection ranges • Of limited diagnostic value	• High throughput • Visual; quantitative	10-12
Purified cell lysate-based approaches			
Mass spectrometry	• Virtually impossible to analyse intact molecules • Challenging data-interpretation due to glycan complexity, proton/cation exchange and loss of sulfo groups • Limited availability of computer assisted programs for complexity analysis	• High-throughput • Confirmatory	13-14
NMR	• Inability to distinguish isomers • Laborious and time consuming method of sample preparation • Loss of surface sugars mainly O-linked along with some N-linked glycans during sample preparation • Inability to analyse whole cells and live cell • Costly instrumentation		

Table 1: Comparison of state-of-the-art technologies for glycoanalysis

No. Of Lectins	Lectins	No. of Elutions	Elutions	No. of Cells	No. of Trenches on Chip
2	LCA, ECL	2	Mannose, Galactose	93	6
3	LCA, ConA, NPL	3	Mannose (3x)	108	6
4	LCA, ECL, ConA, WGA	4	Mannose (2x), Galactose, GlcNAc	75	6

Table 2: Summary of Experimental Procedures

Manuscript Figure Captions

Fig. 1 Principles of the Lab in a Trench microfluidic platform: **(a)** Simulation of cell capture based on sedimentation of cells to the bottom of the trench structure [15]. **(b)** Operating principle of the Lab in a Trench platform. Reagents are exchanged by diffusion permitting a shear-free environment at the bottom of the trench structure.

Fig. 2 Series of images of sequential elution of fluorophore-labelled lectin off Ramos cells: Images **i, ii, iii** show diffusion of LCA into the channel and staining of the cells after 0, 5, 10 minutes. Image **iv** shows the cells after free mannose had been diffused into the system. Image **v** was taken after ECL had been added to the system.

Fig. 3 (a) Average intensity of individual cell staining as calculated by ImageJ. Each lectin and elution step is represented by an individual colour. Each step within each colour on the plot represents a 5-minute time interval. Images collected at 5-minute intervals after addition of LCA (Blue), mannose (red), ECL (green) and lactose (purple). **(b)** An example of a cell stained sequentially with LCA and ECL, and resulting overlay. **(c)** Average peak intensity values of individual cell staining.

Fig. 4 (a) Average intensity of individual cell staining as calculated by ImageJ. Each lectin and elution step is represented by an individual colour. Each step within each colour on the plot represents a 5-minute interval. The images were collected at 5-minute intervals after addition of LCA (Blue), ConA (green), NPL (purple) and mannose (red). **(b)** An example of a cell sequentially stained with LCA, ConA and NPL and resulting overlay. **(c)** Average peak intensity values of individual cell staining.

Fig. 5 (a) Each lectin and elution step is represented by a distinct colour. Each step within each colour on the plot represents a 5-minute time interval. Sequential Profile Steps (5-Minute Intervals): LCA (lectin-Blue), mannose (elution-Red), ECL (lectin-Green), galactose (elution-Orange), ConA (lectin-Purple), mannose (elution-Red), WGA (lectin-Brown), GlcNAc (elution-Black). **(b)** An example of a cell sequentially stained with LCA, ECL, ConA and WGA and resulting images overlaid. **(c)** Average peak intensity values of individual cell staining.

Supplementary Figure Captions

Supplementary Fig. 1: Flow-cytometry based benchmarking data.

Supplementary Fig. 2: (a) ImageJ-based qualitative analysis for identifying sugar distribution profiles on the cell surface. LCA-based mannose probing was performed. The pixilated image with bright patches corresponds to high density of mannose; dark patches show reduced mannose in that part of cell for binding to LCA lectin. (b) Co-localization of galactose (ECL) and mannose (LCA) sugars as a function of their lectin-binding profiles. This qualitative information can be employed for designing further studies, such as identifying sugar locations on the signalling domains present on cell surface.

Supplementary Fig. 3: Relative positioning of sugars. The overlaps were performed between all the sugars but these are representative overlaps of the mentioned pairs. Colour codes for sugars are ConA-cyan, ECL-green, LCA-blue, and WGA-magenta (Figure 1; main text). Cyan and magenta overlaps shows white patches, which are actually overlapping of ConA and WGA while the location where they are not overlapping can be seen as individual colours. This demonstrates that overlaps can be used to map sugar sequences qualitatively where exact measurements are not anticipated.

Supplementary Fig. 4: NPL healthy vs apoptotic cells. Apoptosis was induced by anti-IgM treatment for 24 hours. NPL probing was performed for identification of mannose residues.

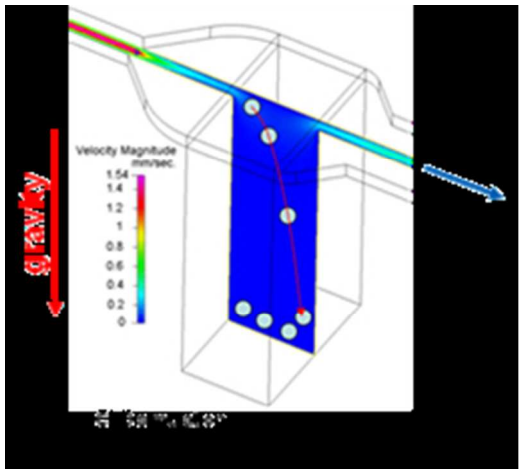

130x117mm (50 x 50 DPI)

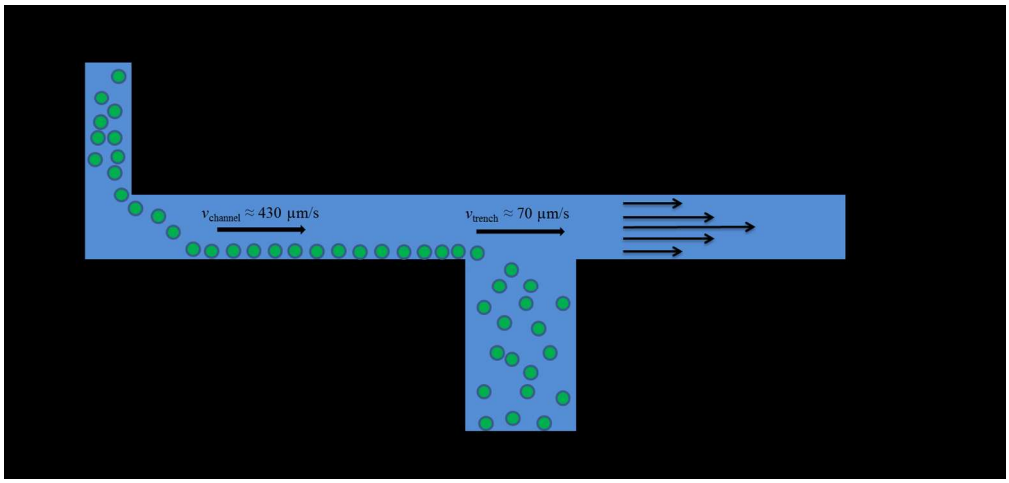

302x143mm (150 x 150 DPI)

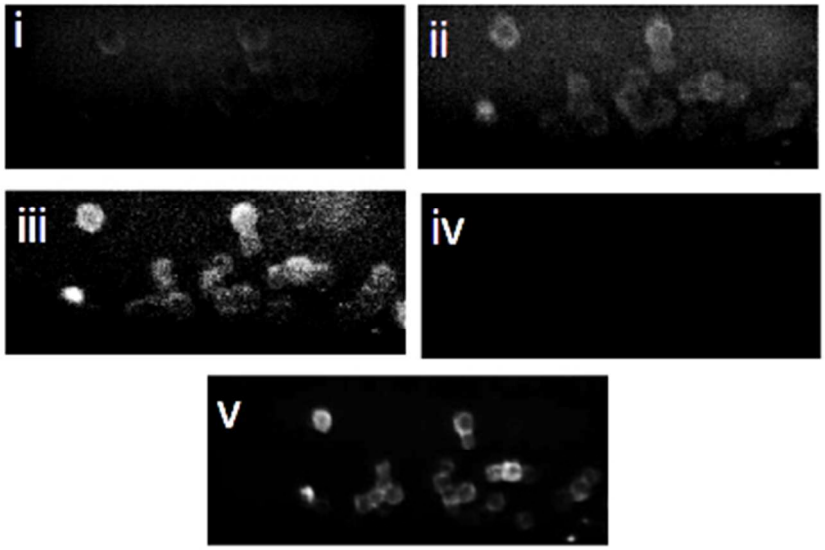

49x34mm (220 x 220 DPI)

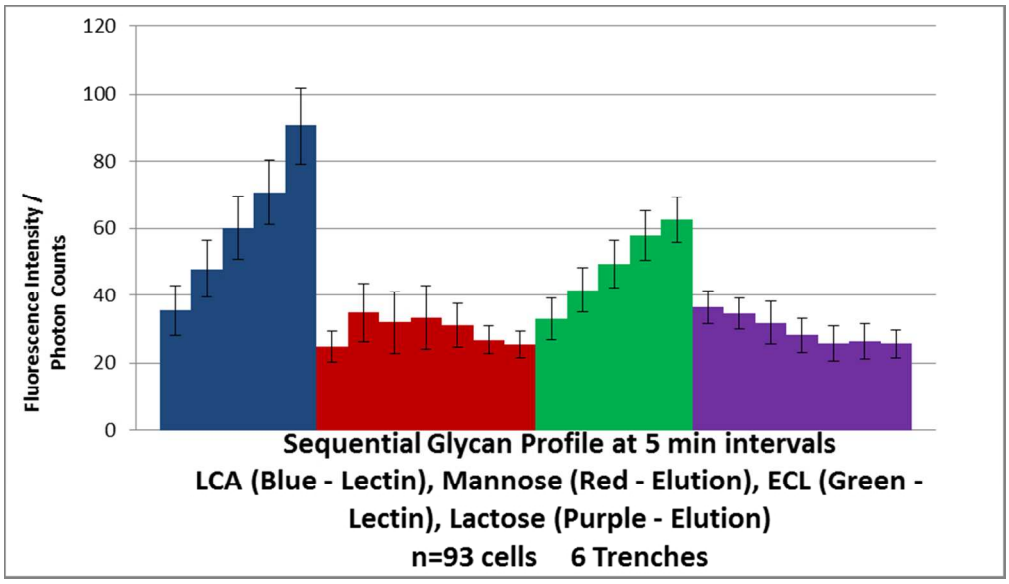

159x91mm (150 x 150 DPI)

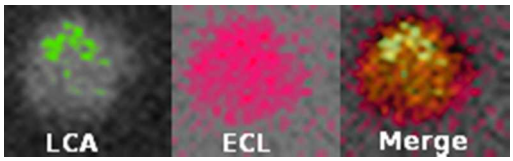

88x26mm (72 x 72 DPI)

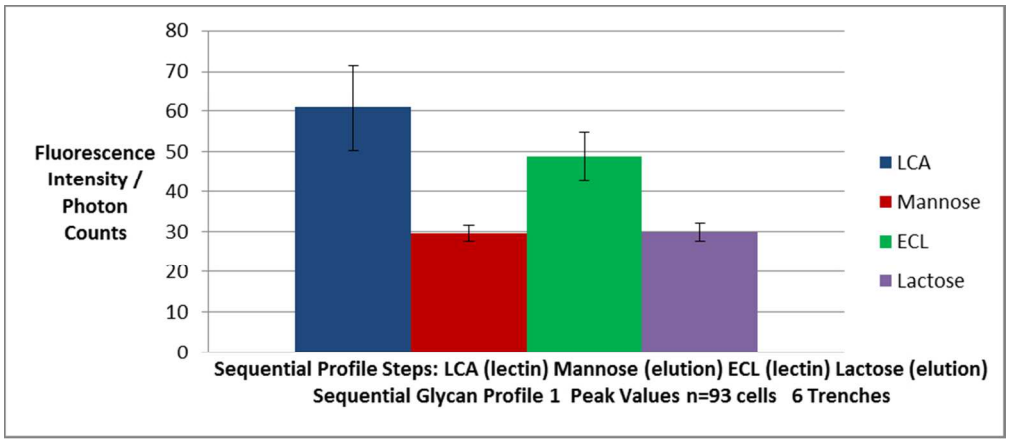

159x69mm (150 x 150 DPI)

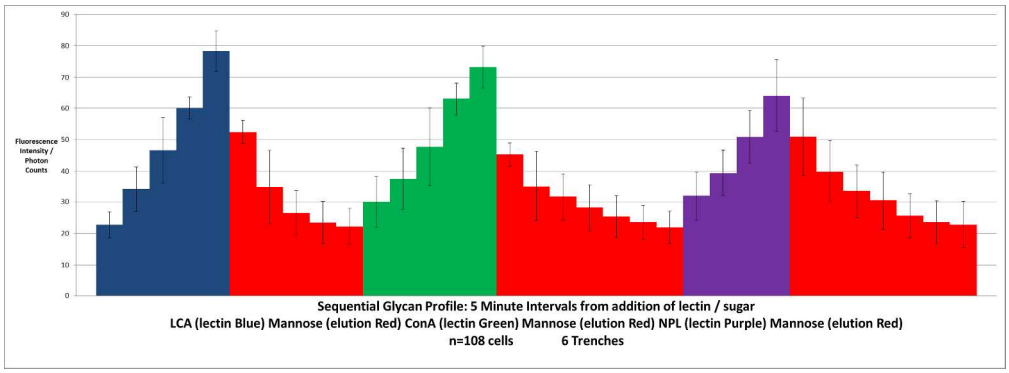

452x164mm (150 x 150 DPI)

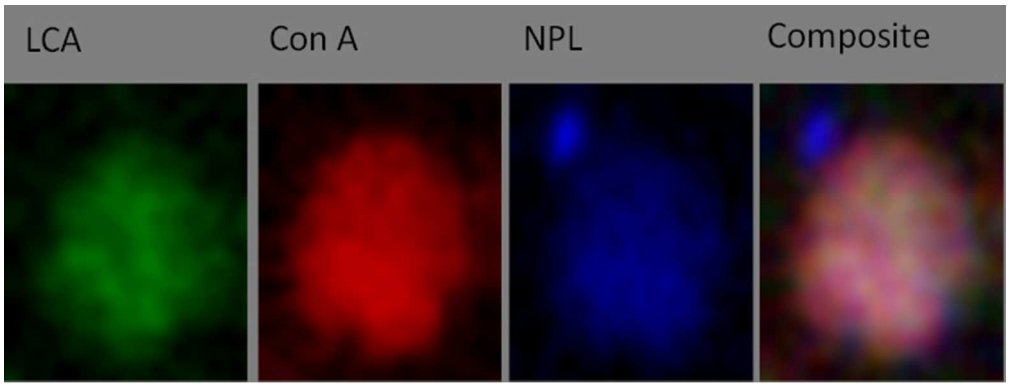

187x70mm (96 x 96 DPI)

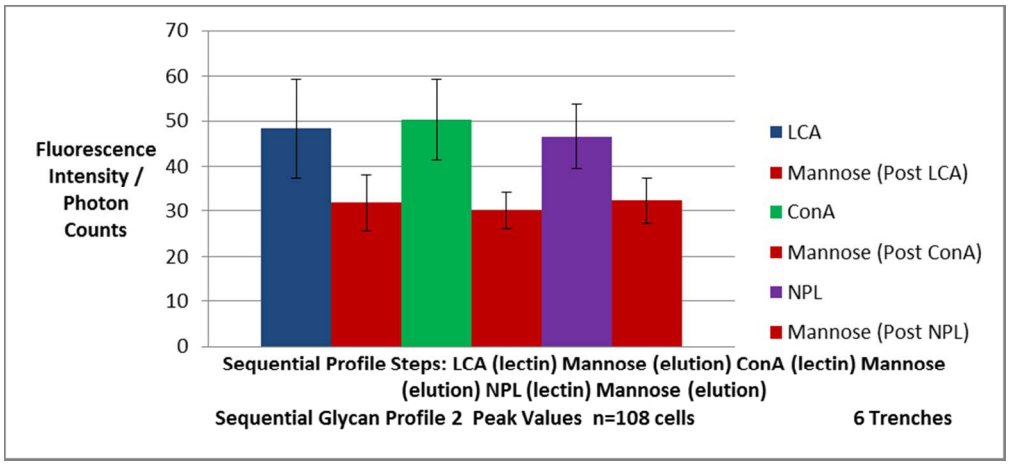

159x72mm (150 x 150 DPI)

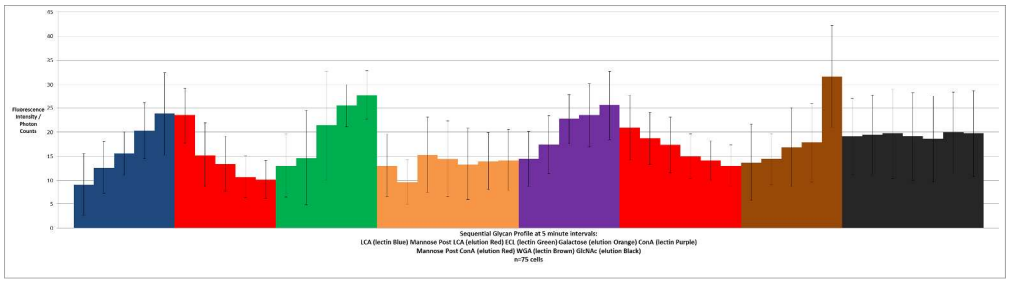

600x164mm (150 x 150 DPI)

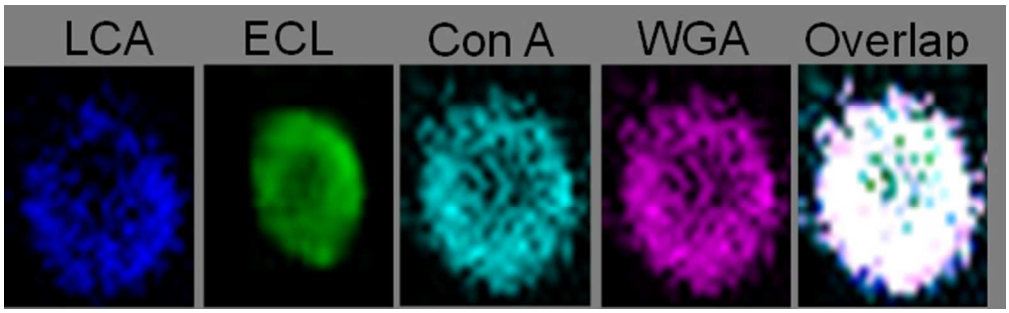

179x54mm (96 x 96 DPI)

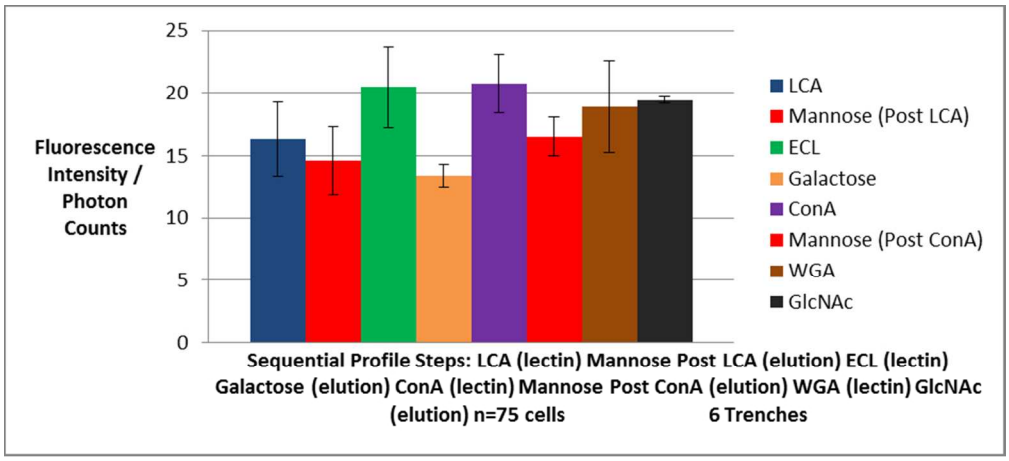

159x71mm (150 x 150 DPI)